

Quantum oscillations in the microwave magnetoabsorption of a 2D electron gas.

O. M. Fedorych,¹ M. Potemski,¹ S. A. Studenikin,² J. A. Gupta,² Z. R. Wasilewski,² and I. A. Dmitriev^{3,*}

¹*Grenoble High Magnetic Field Laboratory, CNRS, Grenoble, France*

²*Institute for Microstructural Sciences, NRC, Ottawa, Ontario K1A-0R6, Canada*

³*Institute of Nanotechnology, Karlsruhe Institute of Technology, 76021 Karlsruhe, Germany*

(Dated: November 2, 2018)

We report on the experimental observation of the quantum oscillations in microwave magnetoabsorption of a high-mobility two-dimensional electron gas induced by Landau quantization. Using original resonance-cavity technique, we observe two kinds of oscillations in the magnetoabsorption originating from inter-Landau-level and intra-Landau-level transitions. The experimental observations are in full accordance with theoretical predictions. Presented theory also explains why similar quantum oscillations are not observed in transmission and reflection experiments on high-mobility structures despite of very strong effect of microwaves on the dc resistance in the same samples.

PACS numbers: 73.50.Jt; 73.40.-c; 78.67.-n; 78.20.Ls; 73.43.-f

Quantum oscillations in absorption (QMA) by a two-dimensional electron gas (2DEG) in perpendicular magnetic field B , governed by the ratio ω/ω_c of the wave frequency $\omega = 2\pi f_{\text{mw}}$ of external electro-magnetic wave and the cyclotron frequency $\omega_c = eB/mc$, were predicted long ago by Ando¹ and observed experimentally² in the IR-absorption on a low-mobility and high-density 2DEG in a Si-inversion layer. Recently, similar ω/ω_c -oscillations were discovered in the dc resistance of a high-mobility 2DEG irradiated by microwaves.³ Particularly intriguing are zero-resistance states⁴ which develop in the minima of these microwave-induced resistance oscillations (MIRO).

Theoretically, both MIRO (Refs. 5–7) and QMA (Refs. 1,5–8) stem from microwave-assisted transitions between disorder-broadened Landau levels (LLs). However, in experiments on high-mobility samples no QMA were observed so far despite strong MIRO showing up in the same experimental conditions. Several attempts to measure microwave reflection or transmission simultaneously with MIRO reported either single cyclotron resonance (CR) peak^{9–11} or more complex structure dominated by confined magnetoplasmons (CMP).^{12–14}

Using original resonance-cavity technique, in this work we observe well-pronounced QMA in a high-mobility GaAs/AlGaAs sample which also reveals strong MIRO in dc transport measurements. For both the T -independent QMA and dynamic Shubnikov-de Haas oscillations (SdHO), the experimental results fully agree with the theoretical predictions of Ref. 5, which generalizes theory¹ of Ando for the case of smooth disorder potential appropriate for high-mobility structures. In addition, we explain the failure to observe such quantum oscillations in transmission and reflection experiments.

We start with a summary of relevant theoretical results which includes QMA theory⁵ for dynamic conductivity at high LLs and nonlinear relation between the absorption and dynamic conductivity^{8,10,15} specific for high-mobility 2DEG samples. Consider a plane wave normally incident to the 2DEG at the interface $z = 0$ between two dielectrics with permittivity ϵ_1 ($z < 0$) and ϵ_2 ($z > 0$). The electric field $\text{Re}\mathbf{E}_l$ of external ($l = e$),

reflected ($l = r$), and transmitted ($l = t$) waves is a real part of $\mathbf{E}_l = \mathcal{E}_l \exp(ik_l z - i\omega t) \sum_{\pm} s_{\pm}^{(l)} \mathbf{e}_{\pm}$, where the wave numbers $k_e/\sqrt{\epsilon_1} = -k_r/\sqrt{\epsilon_1} = k_t/\sqrt{\epsilon_2} = \omega/c$, coefficients $s_{\pm}^{(l)}$ describe the polarization, $\sum_{\pm} |s_{\pm}^{(l)}|^2 = 1$, and $\sqrt{2}\mathbf{e}_{\pm} = \mathbf{e}_x \pm i\mathbf{e}_y$. According to the Maxwell equations, boundary conditions at $z = 0$ read $\mathbf{E}_t = \mathbf{E}_r + \mathbf{E}_e$ and $\partial_z(\mathbf{E}_t - \mathbf{E}_r - \mathbf{E}_e) = (4\pi/c^2) \partial_t \hat{\sigma}\mathbf{E}_t$. It follows that

$$\sqrt{\epsilon_1}\mathcal{E}_e s_{\pm}^{(e)}/\mathcal{E}_t s_{\pm}^{(t)} = \sqrt{\epsilon_{\text{eff}}} + 2\pi\sigma_{\pm}/c, \quad (1)$$

where $2\sqrt{\epsilon_{\text{eff}}} = \sqrt{\epsilon_1} + \sqrt{\epsilon_2}$. Further, $\sigma_{\pm} = \sigma_{xx} \pm i\sigma_{yx}$ are the eigenvalues of the complex conductivity tensor $\hat{\sigma}$ having the symmetries $\sigma_{xx} = \sigma_{yy}$ and $\sigma_{xy} = -\sigma_{yx}$, namely, $\hat{\sigma}\mathbf{e}_{\pm} = \sigma_{\pm}\mathbf{e}_{\pm}$.

Equation (1) yields the absorption \mathcal{A} , transmission \mathcal{T} , and reflection \mathcal{R} coefficients (see also Refs. 8,10,15),

$$\mathcal{A} = \sum_{\pm} \frac{\sqrt{\epsilon_1} |s_{\pm}^{(e)}|^2}{|\sqrt{\epsilon_{\text{eff}}} + 2\pi\sigma_{\pm}/c|^2} \text{Re} \frac{4\pi\sigma_{\pm}}{c}, \quad (2)$$

$$\mathcal{T} = \sum_{\pm} \frac{\sqrt{\epsilon_1\epsilon_2} |s_{\pm}^{(e)}|^2}{|\sqrt{\epsilon_{\text{eff}}} + 2\pi\sigma_{\pm}/c|^2}, \quad (3)$$

$$\mathcal{R} = \sum_{\pm} |s_{\pm}^{(e)}|^2 \left| \frac{\sqrt{\epsilon_1} - \sqrt{\epsilon_2} - 4\pi\sigma_{\pm}/c}{\sqrt{\epsilon_1} + \sqrt{\epsilon_2} + 4\pi\sigma_{\pm}/c} \right|^2. \quad (4)$$

It is important to mention that the dynamic conductivity σ_{\pm} , which is the focus of present study, is the response to the screened electric field acting on 2D electrons. By contrast, coefficients (2)–(4) represent a response to the (unscreened) electric component of incoming wave and, therefore, measure both single-particle (transport) and collective (screening) properties of 2DEG.

The dynamical screening, represented by the denominators in Eqs. (2)–(4), becomes particularly strong in high-mobility structures where the ratio $|2\pi\sigma_{\pm}/c|$ reaches values much larger than unity. Indeed, in the absence of Landau quantization the conductivity $\sigma_{\pm} = \sigma_{\pm}^D$ is given by the Drude formula,

$$\sigma_{\pm}^D = \frac{ne^2/m}{\tau_{\text{tr}}^{-1} - i(\omega \pm \omega_c)}, \quad (5)$$

where τ_{tr} is the momentum relaxation time. The absorption, Eq. (2), takes the form

$$A^D = \sqrt{\frac{\epsilon_1}{\epsilon_{\text{eff}}}} \sum_{\pm} |s_{\pm}^{(\epsilon)}|^2 \frac{\Omega \tau_{\text{tr}}^{-1}}{(\Omega + \tau_{\text{tr}}^{-1})^2 + (\omega \pm \omega_c)^2}, \quad (6)$$

where $\hbar\Omega = 2\alpha\varepsilon_F/\sqrt{\epsilon_{\text{eff}}}$, $\alpha = e^2/\hbar c \simeq 1/137$ is the fine structure constant, and ε_F is the Fermi energy of 2DEG. In high-mobility 2DEG $\Omega\tau_{\text{tr}} \gg 1$ and the width of the cyclotron peak in Eqs. (2)–(4) and (6) is dominated by strong reflection of microwaves. In the region $|\omega - \omega_c| \lesssim \Omega$, where $|2\pi\sigma_-| \gg c$, the collective effects are pronounced. In this region, a special care should be taken to avoid the finite-size magnetoplasmon effects.^{12–14}

According to Ref. 5 (which generalizes the results of Ref. 1 for the relevant case of smooth disorder potential, see also Refs. 7 and 8), Landau quantization at high LLs modifies Drude formula to the form which we call the quantum Drude formula (QDF) in what follows,

$$\text{Re}\sigma_{\pm} = \frac{ne^2}{\omega m} \int \frac{d\varepsilon (f_{\varepsilon} - f_{\varepsilon+\omega}) \tilde{\nu}(\varepsilon) \tau_{\text{tr},\text{B}}^{-1}(\varepsilon + \omega)}{[\tau_{\text{tr},\text{B}}^{-2}(\varepsilon) + \tau_{\text{tr},\text{B}}^{-2}(\varepsilon + \omega)]/2 + (\omega \pm \omega_c)^2}. \quad (7)$$

where f_{ε} is the Fermi distribution function. The Landau quantization leads to the oscillatory density of states (DOS), $\nu(\varepsilon) = \nu(\varepsilon + \omega_c) \equiv \nu_0 \tilde{\nu}(\varepsilon)$, and to renormalization of the transport relaxation time, $\tau_{\text{tr},\text{B}}(\varepsilon) \equiv \tau_{\text{tr}} \tilde{\nu}(\varepsilon)$, where $\nu_0 = m/2\pi\hbar^2$ is the zero- B DOS per spin orientation. In the limit of strongly overlapping LLs, $\omega_c\tau_q \ll 1$, where τ_q is the quantum relaxation time, the DOS is weakly modulated by magnetic field,

$$\tilde{\nu}(\varepsilon) = 1 - 2\delta \cos \frac{2\pi\varepsilon}{\omega_c}, \quad \delta = e^{-\pi/\omega_c\tau_q} \ll 1. \quad (8)$$

In the opposite limit $\omega_c\tau_q \gg 1$, LLs become separated, $\tilde{\nu}(\varepsilon) = \tau_q \text{Re}\sqrt{\Gamma^2 - (\varepsilon - \varepsilon_n)^2}$, where $\Gamma = \sqrt{2\omega_c/\pi\tau_q} < \omega_c/2$, and ε_n marks the position of the nearest LL.

At the CR $\omega = \omega_c$, QDF (7) reads

$$\sigma_-|_{\omega_c=\omega} = \sigma_-^D|_{\omega_c=\omega} \int d\varepsilon \Theta[\nu(\varepsilon)] \frac{f_{\varepsilon} - f_{\varepsilon+\omega}}{\omega}, \quad (9)$$

where the integration is over the regions with $\nu(\varepsilon) > 0$. In the case of overlapping LLs, this produces the classical Drude result $\sigma_- = \sigma_-^D$ meaning that quantum effects in the vicinity of the resonance are absent. In the case of separated LLs, $\omega_c \gg \Gamma$, the conductivity is reduced, $\sigma_-|_{\omega_c=\omega} = (2\Gamma/\omega_c)\sigma_-^D$. At the same time, the CR width increases from τ_{tr}^{-1} to $\tau_{\text{tr}}^{-1}\omega_c/\Gamma$.^{5,16}

In what follows we consider the region $|\omega - \omega_c| \gg \tau_{\text{tr}}^{-1}$ where one can safely neglect τ_{tr}^{-1} in the denominator of Eq. (6) and QDF, Eq. (7), which gives

$$A/A^D = \int d\varepsilon \frac{f_{\varepsilon} - f_{\varepsilon+\omega}}{\omega} \tilde{\nu}(\varepsilon) \tilde{\nu}(\varepsilon + \omega). \quad (10)$$

Equation (10) is the key theoretical result for our study. It expresses the imbalance between the rates of absorption and emission of the microwave quanta, both proportional to the product of initial and final density of states.

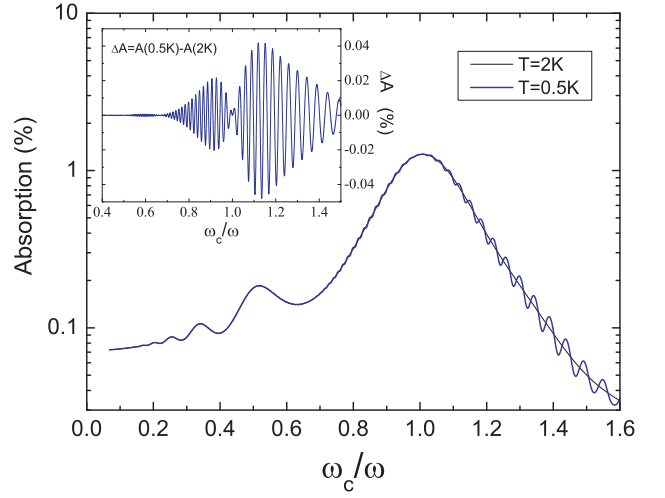


FIG. 1: Magnetoabsorption calculated using Eqs. (10) and (6) for two temperatures $T=2$ K and 0.5 K. Frequency $f_{\text{mw}}=60$ GHz, density $n = 1.8 \cdot 10^{11} \text{cm}^{-2}$, mobility $\mu = 10^7 \text{cm}^2/\text{Vs}$, and $\tau_q = 15$ ps. The difference between traces at $T=0.5$ K and 2 K in the inset shows the T -dependent dynamic SdHO.

The screening properties of a 2DEG at $|\omega \pm \omega_c| \gg \tau_{\text{tr}}^{-1}$ are solely determined by the non-dissipative part of conductivity, $\text{Im}\sigma_{\pm} \simeq ne^2/m(\omega \pm \omega_c) \gg \text{Re}\sigma_{\pm}$, which remains finite at $\tau_{\text{tr}}^{-1} \rightarrow 0$. That is why the transmission and reflection coefficients, Eqs. (3) and (4), in high-mobility structures are almost independent of disorder scattering making it very difficult to observe QMA in direct transmission and reflection experiments.^{9–13}

Magnetoabsorption at two temperatures $T=2$ K and 0.5 K as given by Eqs.(6) and (10) is illustrated in Fig. 1 for high-mobility 2DEG similar to best structures used for MIRO measurements. The broadening of the envelope Drude peak (6) is dominated by strong reflection of microwaves near the CR since in our example $\Omega \sim \omega \gg \tau_{\text{tr}}^{-1}$. The Drude peak in Fig. 1 is modulated by the dynamic SdHO (at $\omega_c \gtrsim \omega$ and $T=0.5$ K) and by the temperature-independent QMA with maxima at the CR harmonics $\omega = N\omega_c$, which we discuss below.

At low temperature, $X_T = 2\pi^2 T/\hbar\omega_c \lesssim 1$, the absorption (10) manifests the dynamic SdHO, which in the case of overlapping LLs (8) are given by

$$A/A^D = 1 - \frac{4X_T\delta}{\sinh X_T} \frac{\omega_c}{2\pi\omega} \sin \frac{2\pi\omega}{\omega_c} \cos \frac{2\pi\varepsilon}{\omega_c}. \quad (11)$$

The dynamic SdHO are exponentially suppressed at $X_T \gg 1$ similar to SdHO in the dc resistance. In the inset it is clearly seen that the dynamic SdHO are periodically modulated according to $\sin(2\pi\omega/\omega_c)$ with nodes at the CR harmonics.

At $e^{-X_T} \ll \delta$, i.e. $T \gg T_D = \hbar/2\pi\tau_q$, SdHO (11) become exponentially smaller than T -independent ω/ω_c -oscillations of second order $\mathcal{O}(\delta^2)$ which represent QMA,

$$A/A^D \simeq \langle \tilde{\nu}(\varepsilon) \tilde{\nu}(\varepsilon + \omega) \rangle = 2\delta^2 \cos \frac{2\pi\omega}{\omega_c}. \quad (12)$$

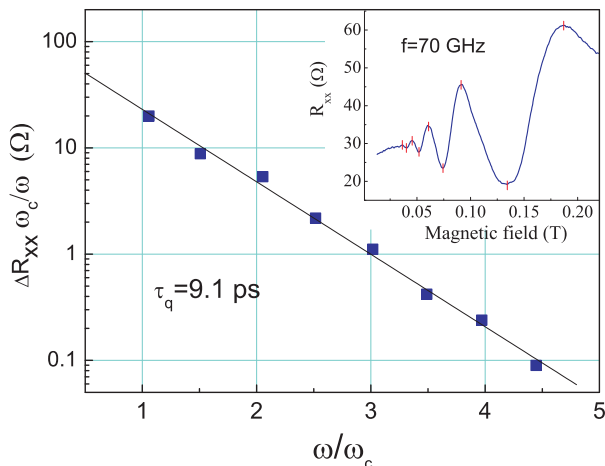


FIG. 2: MIRO measured on Sample 1 for $f_{\text{mw}} = 67$ GHz at $T = 2$ K (inset), and the amplitude of MIRO vs. ω/ω_c in semi-log scale (main panel). The linear fit yields the quantum scattering time $\tau_q = 9.1$ ps, see Eqs. (13) and (8).

Here the angular brackets denote ε -averaging over the period ω_c . Maxima of QMA seen in Fig. 1 appear at integer harmonics of the CR $\omega/\omega_c = N$. The amplitude of QMA (12) becomes of order unity when the DOS modulation is pronounced, i.e. $\delta \sim 1$.¹⁷

Since QMA lie in the microscopic origin of MIRO⁵, it is instructive to compare the expression (12) to results for MIRO in the same regime. For inelastic mechanism of MIRO^{5,6}, the photoresistivity ρ_{ph} in terms of Drude resistivity ρ^D reads

$$\frac{\rho_{\text{ph}}}{\rho^D} = 1 + 2\delta^2 - \frac{4\tau_{\text{in}}\mathcal{P}^D}{\omega^2\nu_0}\delta^2 \frac{2\pi\omega}{\omega_c} \sin \frac{2\pi\omega}{\omega_c}. \quad (13)$$

where the microwave power dissipated in the absence of Landau quantization is $\mathcal{P}^D = \mathcal{A}^D \sqrt{\epsilon} \tau_{\text{in}} E_e^2 / 4\pi$, and τ_{in} is the inelastic relaxation time. Below we use Eq. (13) to determine τ_q from dc measurement of MIRO. The known value of τ_q enables a direct comparison of the measured and calculated QMA [Eq. (12)] without fitting parameters.

Experiment. Two rectangular samples were cleaved from a single MBE-grown wafer of a high-mobility GaAs/AlGaAs heterostructure V0050. After illumination with red light the electron concentration was $n = 3.6 \times 10^{11} \text{cm}^{-2}$ and mobility $\mu = 5 \times 10^6 \text{cm}^2/\text{Vs}$. Sample 1 was prepared for dc transport measurements. In-Sn Ohmic contacts were made by rapid annealing in reducing atmosphere of argon bubbled through hydrochloric acid. The sample was placed in a helium cryostat equipped with a superconducting magnet. Similar to Refs. 10 and 12, microwaves from an HP source, model E8257D, were delivered to the sample using Cu-Be coaxial cable terminated with a 3 mm antenna.

Inset in Fig. 2 shows dc resistance R_{xx} measured in sample 1 at $f_{\text{mw}} = 70$ GHz and $T = 2$ K which displays well resolved MIRO. Main panel in Fig. 2 presents the

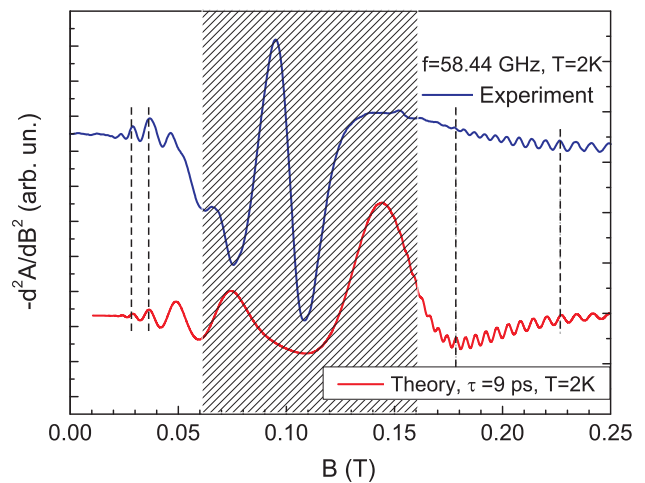


FIG. 3: Magneto-absorption measured on Sample 2 at $T = 2$ K for $f_{\text{mw}} = 58.44$ GHz (top curve) and absorption coefficient \mathcal{A} [Eqs. (10) and (6), bottom curve] calculated without fitting parameters using $\tau_q = 9.1$ ps determined from MIRO measurements on Sample 1 (Fig. 2).

dependence of $\log_{10}(\Delta R_{xx}\omega_c/\omega)$ vs. ω/ω_c , where ΔR_{xx} is the amplitude of MIRO measured between adjacent peaks and dips. In accordance with Eq. (13) containing $\delta^2 = \exp(-2\pi/\omega_c\tau_q)$, this dependence is linear. The slope gives the quantum relaxation time $\tau_q = 9.1$ ps which we use for calculation of QMA in sample 2.

Sample 2 was cleaved from the same wafer in vicinity to sample 1. In order to reduce the CMP effects^{14,15,18}, which can obscure weak QMA oscillations under the investigation, we cleaved a narrow $0.5 \text{ mm} \times 1.5 \text{ mm}$ rectangular stripe. The magneto-absorption experiment was performed using a home-built microwave cavity setup at liquid helium temperatures.¹⁹ The cavity with a tunable resonance frequency had a cylindrical shape with 8 mm diameter and the height between 3 and 8 mm adjustable with a movable plunger. The cavity operated in TE_{011} mode, where $\{011\}$ are the numbers of half-cycle variations in the angular, radial, and longitudinal directions, respectively. The 2DEG stripe was placed at the bottom of the cavity with the external magnetic field normal to the 2DEG plane and the microwave electric field of the TE_{011} mode oriented along the short side of the rectangular sample. The sample was placed in a “face up” fashion such that the active 2DEG layer is separated from the plunger surface by the substrate. This geometry has higher sensitivity to weak absorption signals such as QMA but is not appropriate to study i.e. CMPs in the vicinity of the CR due to cavity over-coupling effects. To further improve sensitivity we measure the differential signal with respect to magnetic field.

The top curve in Fig. 3 presents B dependence of the second derivative of the measured absorption for $f_{\text{mw}} = 58.44$ GHz whereas the bottom curve shows the second B derivative of the absorption coefficient \mathcal{A} , Eqs. (6) and (10), calculated without fitting parameters using

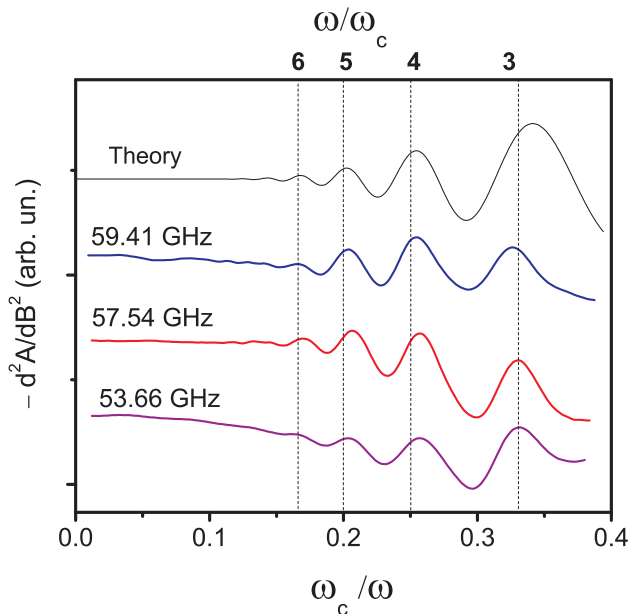


FIG. 4: QMA measured at different frequencies compared to the theory [Eq. (12), parameters as in Fig. 3].

$\tau_q = 9.1$ ps determined from MIRO measurements on sample 1 (Fig. 2). Both curves demonstrate well resolved QMA with maxima at harmonics of the CR and dynamic SdHO with maxima determined by the position of the chemical potential with respect to LLs. Clearly, the theory reproduces the experimental trace in Fig. 3 quite well everywhere except for the shaded region around the CR where the signal is distorted due to the CMP absorption. The dimensions of sample 2 were chosen to allow only one CMP mode at $B = 0.092$ T. The absence of higher modes for $f_{mw} < 63$ GHz enabled the possibility to observe clear

quantum oscillations on both sides of the shaded region where finite-size effects^{14,15,18} are not essential.

The low-field traces ($\omega_c/\omega < 1/2$) of the magnetoabsorption are shown in Fig. 4 for several microwave frequencies together with the function $\delta^2 \cos(2\pi\omega/\omega_c)$. The phase and B damping of the observed QMA follow well the theoretical dependence (12), without fitting parameters. We, therefore, believe that the observed oscillations are indeed QMA predicted in Refs. 1 and 5, which provides an important experimental evidence supporting the theory of MIRO⁵⁻⁷ based on inter-LL transitions. In our sample, QMA are strongly damped [$\delta^2 = 0.02$ at $\omega_c = \omega/2$, $\omega/2\pi = f_{mw} = 58.44$ GHz, and $\tau_q = 9.1$ ps, see Eq. (12)] which makes their observation difficult. We expect that much stronger QMA as well as dynamic SdHO can be observed on samples with higher mobility (longer τ_q), as simulated in Fig. 1, provided the CMP effects are avoided or sufficiently reduced.

In summary, we have observed quantum magnetooscillations in the microwave absorption and dynamic SdHO in a high mobility 2DEG. For this purpose we used a sensitive high- Q cavity technique and developed a special setup to avoid undesirable magnetoplasmon effects masking the quantum oscillations. Using the quantum Drude formula⁵ and the quantum relaxation time extracted from the MIRO measurements on the same wafer we were able to reproduce the experimental results for absorption without fitting parameters, which provides a strong experimental support to the theory of MIRO and QMA based on inter-LL transitions.

We are thankful to A. D. Mirlin, D. G. Polyakov, B. I. Shklovskii, S. A. Vitkalov, and M. A. Zudov for fruitful discussions. This work was supported by the DFG, by the DFG-CFN, by Rosnauka Grant no. 02.740.11.5072, by the RFBR, and by the NRC-CNRS project.

* Also at Ioffe Physical Technical Institute, 194021 St. Petersburg, Russia

¹ T. Ando, J. Phys. Soc. Jpn. **38**, 989 (1975).

² G. Abstreiter, J. P. Kotthaus, J. F. Koch, and G. Dorda, Phys. Rev. B **14**, 2480 (1976).

³ M. A. Zudov, R. R. Du, J. A. Simmons, and J. L. Reno, Phys. Rev. B **64**, 201311(R) (2001), P. D. Ye, L. W. Engel, D. C. Tsui, J. A. Simmons, J. R. Wendt, G. A. Vawter, and J. L. Reno, Appl. Phys. Lett. **79**, 2193 (2001).

⁴ R. G. Mani, J. H. Smet, K. von Klitzing, V. Narayana-murti, W. B. Johnson, and V. Umansky, Nature **420**, 646 (2002), M. A. Zudov, R. R. Du, L. N. Pfeiffer, and K. W. West, Phys. Rev. Lett. **90**, 046807 (2003).

⁵ I. A. Dmitriev, A. D. Mirlin, and D. G. Polyakov, Phys. Rev. Lett. **91**, 226802 (2003).

⁶ I. A. Dmitriev, M. G. Vavilov, I. L. Aleiner, A. D. Mirlin, and D. G. Polyakov, Phys. Rev. B **71**, 115316 (2005).

⁷ M. G. Vavilov and I. L. Aleiner, Phys. Rev. B **69**, 035303 (2004).

⁸ O. E. Raichev, Phys. Rev. B **78**, 125304 (2008).

⁹ J. H. Smet, B. Gorshunov, C. Jiang, L. Pfeiffer, K. West, V. Umansky, M. Dressel, R. Meisels, F. Kuchar, and K. von Klitzing, Phys. Rev. Lett. **95**, 116804 (2005).

¹⁰ S. A. Studenikin, M. Potemski, A. Sachrajda, M. Hilke, L. N. Pfeiffer, and K. W. West, Phys. Rev. B **71**, 245313 (2005).

¹¹ L. C. Tung, C. L. Yang, D. Smirnova, L. N. Pfeiffer, K. W. West, R. R. Du, and Y.-J. Wang, Solid State Commun. **149**, 1531 (2009).

¹² S. A. Studenikin, M. Potemski, A. S. Sachrajda, M. Hilke, L. N. Pfeiffer, K. W. West, IEEE Trans. Nanotechnol. **4**, 124 (2005).

¹³ A. Wirthmann, B. D. McCombe, D. Heitmann, S. Holland, K.-J. Friedland, and C.-M. Hu, Phys. Rev. B **76**, 195315 (2007).

¹⁴ S. A. Studenikin, A. S. Sachrajda, J. A. Gupta, Z. R. Wasilewski, O. M. Fedorych, M. Byszewski, D. K. Maude, M. Potemski, M. Hilke, K. W. West, and L. N. Pfeiffer, Phys. Rev. B **76**, 165321 (2007).

¹⁵ K. W. Chiu, T. K. Lee, and J. J. Quinn, Surf. Sci. **58**, 182

- (1976).
- ¹⁶ M. M. Fogler and B. I. Shklovskii, *Phys. Rev. Lett.* **80**, 4749 (1998).
- ¹⁷ Resonant features at overtones of CR can be induced by the quasiclassical memory effects even in the absence of Landau quantization, $\delta \rightarrow 0$ [see I. A. Dmitriev, A. D. Mirlin, and D. G. Polyakov, *Phys. Rev. B* **70**, 165305 (2004)]. These classical oscillations originate from the non-Markovian memory effects in the presence of both long-range and short-range randomness in the static impurity potential. The predicted phase of classical oscillations in the dynamic conductivity (and therefore in the absorption coefficient) is opposite to the phase of quantum oscillations (12) while the amplitude can be comparable to the value of Drude conductivity.
- ¹⁸ O. M. Fedorych, S. A. Studenikin, S. Moreau, M. Potemski, T. Saku, Y. Hirayama, *Int. J. Mod. Phys. B* **23**, 2698 (2009).
- ¹⁹ M. Seck and P. Wyder, *Rev. Sci. Instrum.* **69**, 1817 (1998).